



Predicted mechanical performance of pultruded FRP material under severe temperature duress



Behzad Ghadimi^{a,*}, Salvatore Russo^b, Michele Rosano^a

^a Curtin University, Australia

^b Università Iuav di Venezia, Italy

ARTICLE INFO

Article history:

Received 3 February 2017

Revised 5 May 2017

Accepted 23 May 2017

Available online 31 May 2017

ABSTRACT

Pultruded FRP (fibre reinforced polymer) materials have attracted the attention of civil engineers with their high strength weight ratio and environmentally friendly production and use. Mechanical analysis of pultruded FRP profiles is complex since the material is anisotropic and becomes more complex when thin FRP dedicated hollow cross sections are involved. This is particularly relevant with square or rectangular construction forms where the corners of the material are suspected to produce weak points under compressive loading. FRPs are also believed to behave contrarily when subjected to heat and thermal duress. This research investigates problems in predicting their behaviour under compression (hollow square pultruded FRP sample) using different analytical and modelling approaches. The mechanical behaviour of the material is investigated under different thermal conditions through finite element simulation and the results are then compared with previously conducted laboratory research analysis. The large deformation in anisotropic materials is simulated to provide better prediction regarding the failure mechanism of this material. Finite element simulation is then used to estimate the performance of similar and often competitive construction materials to GFRP (i.e.: wood, concrete and steel) under similar thermal and compressive duress.

© 2017 Elsevier Ltd. All rights reserved.

1. Introduction

The use of innovative materials in construction has long been investigated [1]. The issues of material sustainability and resilience across different scales of design, from urban cities to individual building construction are also increasingly being investigated [2].

The pressing need to address the maintenance programs associated with construction material use and design, faced with increasing sustainability management pressures [3] is also noted.

Global sustainability challenges are significant and involve a broad array of issues [4] for the construction materials sector including:

- the inherent energy efficiency afforded by the chosen construction materials,
- the embodied energy involved in their production and distribution,
- construction material durability and implications for sustainable design,
- maintenance and life cycle engineering [10–12],

- associated waste policy and public discourse encouraging materials recycling [5],
- enhanced sustainability performance and recycling with industrial waste [6],
- the development of new energy technologies to reduce greenhouse gas emissions, waste heat and overall energy costs [7],
- newly developing business models to assist sustainable development [8], and
- increasing pressures from world population growth and the associated pressures on resource availability [9].

Polymer-based concrete materials are one of the latest generation of construction materials being investigated [1–3,13].

Whilst concrete innovation research and application is very advanced, polymeric concrete materials like FRP, are still being investigated.

RP (fibre reinforced polymer) materials are primarily known for their light weight, strength and durable application in both new and remedial construction [14], with additional application as diaphragms and sheet piles in niche applications [14].

Within FRP materials, pultruded profiles deserve special attention as they can be produced in various shapes and sections similar to metal structures with similar performance, but exhibiting four

* Corresponding author.

E-mail address: Behzad.Ghadimi@curtin.edu.au (B. Ghadimi).

times the weight/strength ratio. The structural mechanical behaviour of FRP, in the static field, and also in dynamic behaviour is now included in regulations, technical recommendations and calculation manuals for corresponding structural design.

Research and application of the long run behaviour of FRP materials in the presence of severe boundary conditions such as fire, extreme temperatures and environmental duress is under investigation [15,16]. In the European market, there are test specifications for FRP materials in relation to their durability [17]. However, further research on the long term benefits of FRP materials, particularly under thermal duress needs to be investigated.

Some experiments have tested the strength, durability and resilience of FRP materials under significant thermal duress with temperature exposures equal to 200 °C [11,12].

Other research has investigated the performance of pultruded FRP material reinforced with glass fibre and polyester resin (40% and 60% respectively) when subjected to temperature cycles with peak values up to 1000 °C and then examined the affected samples under compression testing [12].

In this research, the pultruded GFRP hollow samples were first subjected to thermal duress ranging from 25 °C to 200 °C across seven different scenarios. In each scenario, the samples experienced different numbers of thermal cycles and peaks. Each thermal cycle consisted of 3 h of thermal peaks and then one hour of cooling down. After the thermal treatment, samples were then subjected to compressive loading until their mechanical collapse [11,12].

This paper also compares the simulated long-term performance of FRP- with other traditional construction materials such as wood, concrete and steel, under similar conditions of thermal and compressive duress. The mechanical response of the materials is then compared based on their compressive strength.

The research conclusions highlight some of the limits faced by numerical analysis in predicting the expected behaviour of FRP pultruded material under duress and the need for additional targeted experimental verification and analysis to support numerical simulation analysis.

2. Experimental results

The GFRP samples utilised were hollow square box sections from an original sample of 1000 mm length. The samples were $10 \times 10 \times 10 \text{ cm}^3$ in dimension. They were subjected to seven different scenarios of temperature duress. Both temperature peaks and the number of cooling-heating cycles were varied. A description of these experimental scenarios is presented in Table 1.

A Contherm thermotec 2000 series oven was used to simulate severe temperature conditions in the experiment. Temperature peaks varied from 50 °C to 200 °C and the number of cycles varied from 50 to 200 cycles.

Table 1
GFRP experimental scenarios.

Scenario Number	Description	Average Duration of a Cycle (minutes)
Scenario 1	Control samples without temperature cycles	0
Scenario 2	50 cycles at 50 °C	196.88
Scenario 3	100 cycles at 50 °C	195.35
Scenario 4	200 cycles at 50 °C	199.21
Scenario 5	3 cycles of 100 °C	191.67
Scenario 6	100 cycles of 50 °C and 3 cycles of 150 °C	195.35 194.67
Scenario 7	200 cycles of 50 °C and 3 cycles of 200 °C	199.21 238.67

Samples from each scenario were then subjected to compression tests conducted with a 500 kN Samuel-Denison universal testing machine (UTM). Samples were equipped with Rubicon 825 controller firmware, version 2.34 and interface version 1.84. Strain gauges K-LY4x-10/120 from HBM were utilised to record the time history of the strain development from the start of loading to after collapse in the samples.

Sample crack development was recorded by an 8-channel digital Acoustic emission signal processor, Micro Express-8 AE from MISTRAS (Physical Acoustics Corporation) with data transfer speeds of over 20 megabytes per second. Details on the acoustic emission analysis can be found in [11,12].

Fig. 1 illustrates the results of compressive loading along with the increasing acoustic events from scenario 1 to scenario 7. Based on these seven scenarios, two different governing equations were developed to predict the behaviour of GFRP materials subjected to heating-cooling cycles and varying temperature peaks (Fig. 1-left).

As can be seen in Fig. 1 (also explained in [11,12]) the response of GFRP materials under compressive loads is complex especially when the effects of temperature peaks and temperature cycles are considered. Therefore, in conjunction with the previous experiments, a newly developed finite element methodology is employed in this research to provide further insight into the GFRPs response to thermal duress.

3. Finite element modelling

In this section, a continuum damage mechanics (CDM) approach is applied to simulate the response of the GFRP materials before, during and after the collapse in terms of load-displacement.

CDM considers various kinds of damage to the structure of the composite materials in terms of degradation. The evolution of damage during the loading is then estimated through empirically developed equations which impose additional parameters on the numerical analysis [18].

In this research, the effects of damage from all sources (load, temperature, time, the number of cycles etc.) are mathematically considered as separate modifications in the model. Firstly, the reduction in the stiffness of GFRP. This reduction is represented by a state variable D , calculated as follow [18]:

$$D = 1 - \frac{E}{\hat{E}} \quad (1)$$

where E and \hat{E} have damaged moduli and original moduli respectively. A second modification is the reduction in the effective cross-section area resisting against the induced load. This can be calculated as follow [18]:

$$D = 1 - \frac{A}{\hat{A}} \quad (2)$$

where A and \hat{A} have damaged cross-section and original cross-section respectively. Now, if we assume the original stress-strain relationship to be as follow [18]:

$$\hat{\sigma} = \hat{E}\hat{\varepsilon} \quad (3)$$

This will change in each load increment to the following [18]:

$$\sigma = E\varepsilon \quad (4)$$

Based on the principle of energy equivalence it can be further noted [18]:

$$\sigma : \varepsilon = \hat{\sigma} : \hat{\varepsilon} \quad (5)$$

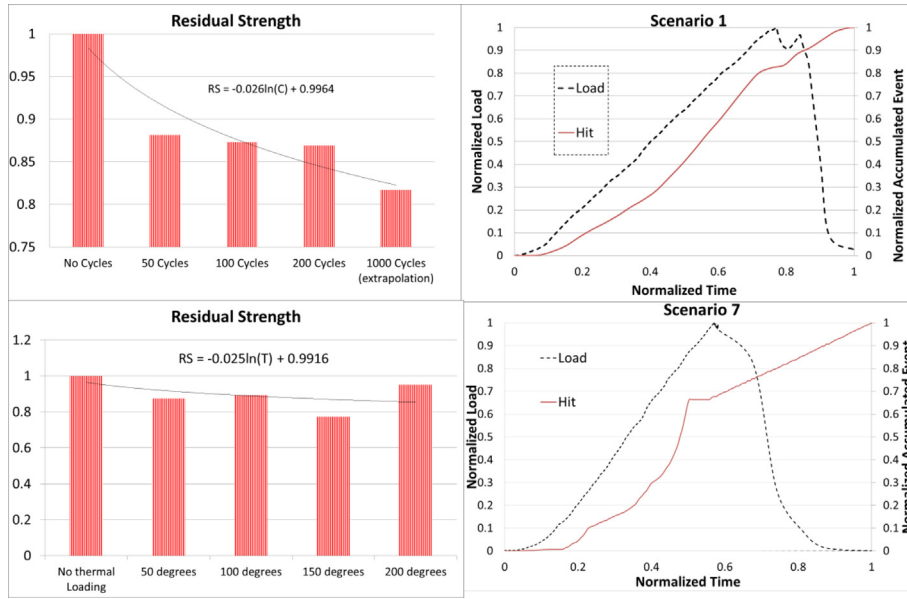


Fig. 1. Experimental results of compressive loading in different scenarios.

where the following two are also applied [1]:

$$\begin{aligned} \sigma &= \hat{\sigma}[1 - D] \\ \hat{\varepsilon} &= \varepsilon[1 - D] \end{aligned} \quad (6)$$

The substitution then yields to the following equation [18]:

$$E(D) = \hat{E}[1 - D] \xrightarrow{\text{yields}} D = 1 - \sqrt{\frac{E}{\hat{E}}} \quad (7)$$

The above equation considers/estimates the modification of the material properties due to the damage incurred. Secondly, the next step required for the analysis is to define the damage threshold and activation function. Damage activation functions can be defined over different variables of stress and strain tensors. In this research, the damage activation function is based on the states of stress and strain tensors as follow [18]:

$$g = \hat{g} - \gamma \leq 0 \quad (8)$$

In this equation g and \hat{g} are the updated and original damage activation function respectively. γ is the updated damage threshold. In this simulation the following activation function and the updated damage threshold is defined as [18]:

$$\begin{aligned} \hat{g} &= f(Rs) \cdot \sqrt{m_1 \frac{Y_2 \hat{E}_2}{U_t^2} + m_2 \left(\frac{Y_2 \hat{E}_2}{U_t^2} \right)^2 + \left(\frac{Y_6 \hat{G}_{12}}{U_s^2} \right)^2} \\ \gamma &= m_3 \exp(\delta) - m_4 \\ Y_2 &= \frac{\sigma_2^2}{(1-D_2)^2 E_2} - \frac{\sigma_1 \sigma_2 \nu_{12}}{(1-D_2)^2 E_1} \\ Y_6 &= \frac{\sigma_6^2}{2(1-D_6)^2 G_{12}} \end{aligned} \quad (9)$$

In the above equations, m_1 , m_2 , m_3 and m_4 are dimensionless material parameters defined by the curve of the collapse of the samples as given in Table 2 [18]. The ultimate tensile and shear strength of the GFRP materials are indicated as U_t and U_s . The Poisson ratio is identified as ?? and ?? is the length of the dry bundle of fibers (10 cm in this simulation) as proposed by Rosen [19]. The subscripts 1,2 and 3 for E , G and ?? are indicators of the direction of the fibres. The strong direction of the composite materials is assumed to be in direction 1 and directions 2 and 3 are orthogonal to direction 1 (weak plane of the materials) [18].

Table 2

GFRP sample material properties.

Property _ GFRP	Notation	Value
Longitudinal tensile modulus of elasticity	E_1	28.5 (GPa)
Transverse tensile modulus of elasticity	$E_2 = E_3$	8.5 (GPa)
Transverse shear modulus of elasticity	G_{23}	3.5 (GPa)
In-plane shear modulus of elasticity	$G_{13} = G_{12}$	2.5 (GPa)
Major Poisson's ratio	$\nu_{12} = \nu_{31}$	0.25
Minor Poisson's ratio	ν_{23}	0.12
Bulk weight density of FRP	γ	1850 (kg/m ³)
Longitudinal tensile strength	σ_{xt}	350 (MPa)
Transverse tensile strength	$\sigma_{yt} = \sigma_{zt}$	70 (MPa)
Longitudinal compressive strength	σ_{xc}	413 (MPa)
Transverse compressive strength	$\sigma_{yc} = \sigma_{zc}$	80 (MPa)
Shear strength	$\tau_{xy} = \tau_{xz} = \tau_{yz}$	40 (MPa)
Dimensionless material parameters	$m1$	0.261
Dimensionless material parameters	$m2$	0.739
Dimensionless material parameters	$m3 = m4$	0.5

The effect of the reduction in strength due to the thermal cycles is reflected through function $f(Rs)$. This function determines the damage activation function value for a specific scenario in which the materials experience specific temperatures and number of thermal cycles.

In this paper, $f(Rs)$ is calculated from the equations initially developed by [11,12]. This function is graphically illustrated in Fig. 2. In this function the residual strength of the GFRP materials (Rs) varies logarithmically with peak temperature (T) and temperature cycles (C) and can be stated in the following equation:

$$Rs = a_1 \text{Log}(C) \text{Log}(T) + a_2 \text{Log}(C) + a_3 \text{Log}(T) + a_4 \quad (10)$$

In this paper the following coefficients are calculated for the material:

- $a_1 = 0.00065$
- $a_2 = 0.025$
- $a_3 = 0.026$
- $a_4 = 1.082$

The four coefficients are related to the trend of compressive strength reduction with the number of thermal cycles and the peak temperature.

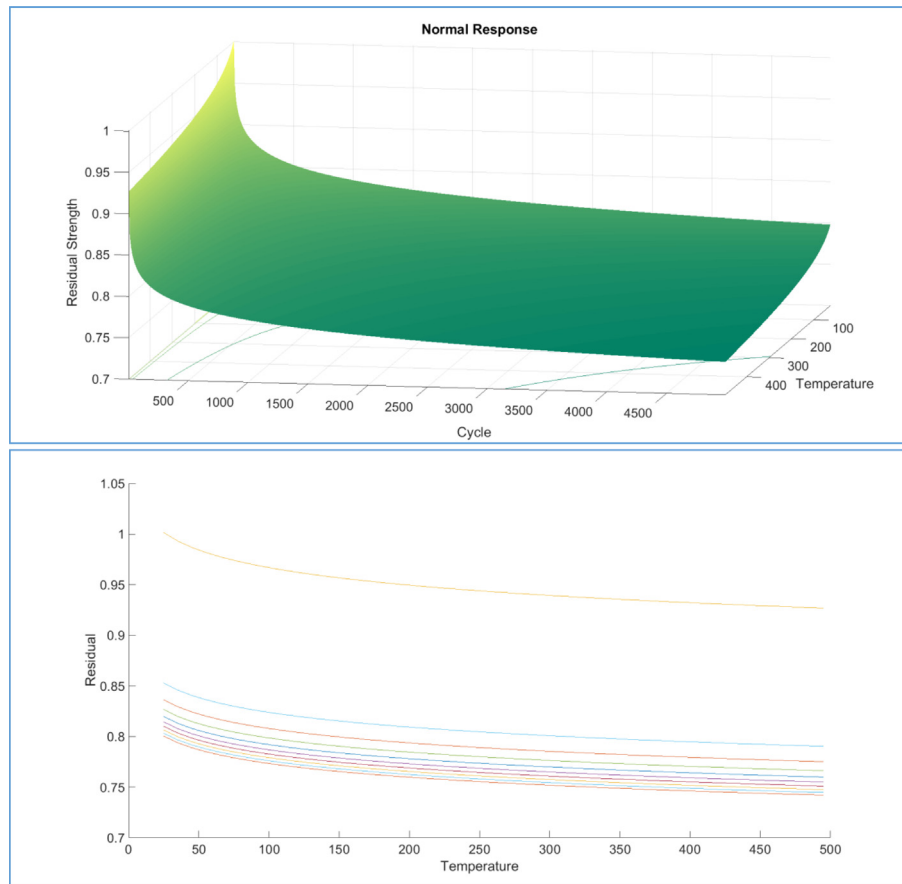


Fig. 2. Variation of Residual strength with temperature peaks and cycles.

Fig. 3 shows the schematic algorithm for the simulation of the CMD model.

Based on this algorithm, the CMD simulation of the GFRP samples is then simulated in an ABAQUS FEM (Finite element model) program.

A square 10×10 cm is meshed with 3400 nodes and 1089 CPS8R plane stress elements. Boundary conditions are clamped at the bottom and roller at the top and sides. To simulate the strain, a controlled experiment, with a maximum of 0.2 mm vertical displacement is applied incrementally to the top edge of the model. Fig. 4 illustrates the finite element mesh to simulate the CMD of GFRPs. The material properties are listed in Table 2. The samples used were hollow square shaped and subjected to uniform compressive loading. The loading and geometry of the sample were symmetrical, therefore, in the simulation only one face of the hollow cube is modelled.

4. Softening behaviour of pultruded GFRP under compressive load

Fig. 5 shows the results of the finite element simulation of the model described in the previous section. In this figure, three different responses are compared: the experimental responses of the sample to the compressive load in each scenario, the finite element simulation of the simple softening model for each scenario and the CDM modelling previously described.

As can be seen from Fig. 5. The CDM model is capable of modelling the complete behaviour of GFRP materials from the linear elastic domain to the collapse and in the post failure region. This

cannot be achieved with simple finite element simulation modelling because the after collapse behaviour produces numerical divergence.

The CDM approach considers material degradation due to the temperature peaks and thermal cycles. Based on the results of this simulation the GFRP becomes more brittle in moving from scenario 1 to scenario 7. This can be seen in the reduction in the area under the load-displacement curve.

In Scenario 1, the CDM predicts a slightly stiffer response from the GFRP. The samples reach 1200 kN and then collapse. The FEM-softening model can simulate the reduction of material strength up to 561 kN and UTM does record a force reduction till 400 kN, whilst the CDM can simulate the materials strength reduction down to 50 kN and below.

In Scenario 2, the CDM predicts a stiffer response from GFRP compared to the recorded response in the experiment. The CDM predicts an ultimate load capacity of 1086 kN whilst in the experiment 1098 kN is recorded.

In Scenario 3, an ultimate load of 1059 kN is predicted and recorded by both the CDM and the experiment. The force-displacement curve shows the softer response from the CDM compared with the experimental results. There is a discrepancy in the simulated response of GFRP with the CDM approach after the collapse load. This is perhaps due to the numerical instability arising from large deformation anisotropic behaviour from samples under compressive load.

In Scenario 4, the ultimate capacity of the materials is predicted to be 1041 kN while in the experiment 1094 kN is recorded. This

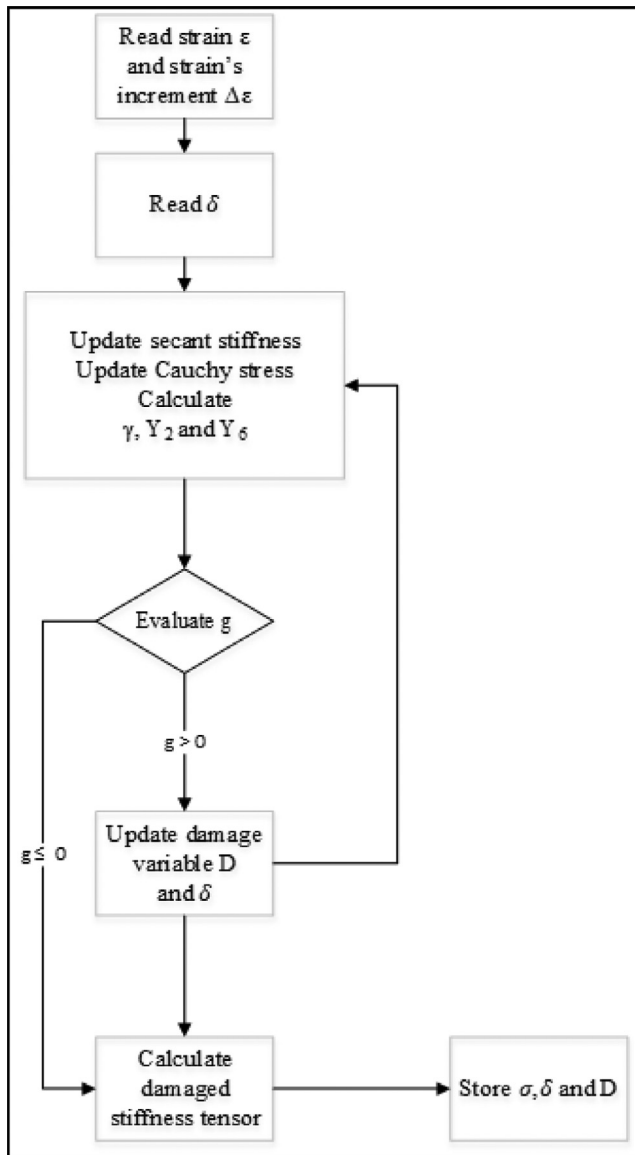


Fig. 3. CMD simulation algorithm.

difference is expected to relate to the out of trend behaviour of the experimental samples in Scenario 4.

In Scenario 5 the ultimate capacity of the samples was experimentally recorded as 1122 kN whilst the CDM calculated 1014 kN as the ultimate capacity.

In Scenario 6 both the experiment and the CDM recorded 972 kN as the ultimate capacity of the samples.

Finally, in Scenario 7 the experiment shows a 1197 kN ultimate capacity whilst only 924 kN is predicted by the CDM. This discrepancy is also expected to be attributed to an out-of-trend behaviour by the samples in Scenario 7. In this scenario, a significant reduction in both stiffness and the ultimate capacity of the materials was expected.

It should be noted that the rate of failure of the samples under compressive testing is higher than the rate of deformation data recorded by the UTM. Therefore, the actual path of the collapse cannot be captured precisely with UTM. As a result, the FEM data should not be entirely disregarded because of its disagreement with experimental data. The actual failure path should have occurred somewhere between these two curves. This matter will be discussed in more detail in Section 8.

5. Simulation of strength degradation in wood due to increasing temperature

Wood has been long used as a building material in the construction industry. Wood is considered to be an orthotropic brittle material and therefore, its mechanical behaviour is similar to GFRP materials. Manriques and Moraes [20] studied the effect of temperature on the compressive strength of wood materials. In this research, the temperature varied between 20 °C and 240 °C. They proposed a polynomial function to predict the residual compressive strength of the wood after thermal duress. This is represented in Fig. 6.

Based on their presented data the following polynomial function has been adopted in this simulation:

$$R_s = 1.9167 \times 10^{-9}T^4 - 1.9732 \times 10^{-6}T^3 + 2.3448 \times 10^{-4}T^2 - 1.7839 \times 10^{-2}T \quad (11)$$

In Eq. (10), the temperature (T) can vary between 20 to 250 °C and the R_s is the residual strength (percentage) of wood.

Table 3 shows wood's material properties used for the purpose of FE simulation.

The original mesh (undeformed) and deformed mesh of the simulation can be seen in the Fig. 7. In this section a hollow square box made of wood is simulated. The box is a cube of $10 \times 10 \times 10$ cm and is modelled by 10,000, S8R 8 nodes shell elements. The model is subjected to uniformly distributed compressive pressure. A static risk method of analysis is described in [11] and [12] and is adopted to simulate the collapse of the wood sample under compressive load.

Fig. 8 shows the results of degrading compressive strength in the wood due to increasing temperature. The plastic rate dependent models previously used in [11] are now updated with Eq. (10). It can be seen that the strength and stiffness of the wood materials decreases noticeably with temperature. The collapse strength decreases from 32 kN at 20 °C to 17 at 200 °C. The simulation modelling showed an increase in the residual strength of the wood after the collapse load which occurred due to the hardening of the material. This is why the ultimate loading capacity of wood is greater than the collapse load.

The stiffness of wood also decreases with an increase in temperature. Fig. 8 illustrates the comparison of the residual strength of the wood materials after being subjected to severe temperature duress. The results of numerical simulation are then developed based on the reported experimental data by Manriques and Moraes [20].

6. Simulation of strength degradation in concrete due to increasing temperatures

To simulate concrete performance, a smeared model has been used. This model can simulate the discontinuous macro cracking observed in concrete materials. Similar to CDM, the presence of cracks affects the stiffness and stress of materials in each increment of calculation. Detail on the equations and approaches utilised in this analysis are presented in [22].

Chen et al. [23] investigated the residual compressive strength of concrete samples with varying temperature. Fig. 9 shows the finite element model simulating their results for normal strength concrete (NSC) along with deformed mesh. The sample is a 10 cm^3 cube consisting of 8000 linear hexahedral solid elements of type C3D8R. This cube is under uniformly distributed compressive load. The strength reduction of NSC samples with temperature according to Chen et al. [23] are represented in Fig. 10.

Eq. (12) is used to predict the residual strength of NSC after being subjected to high temperature:

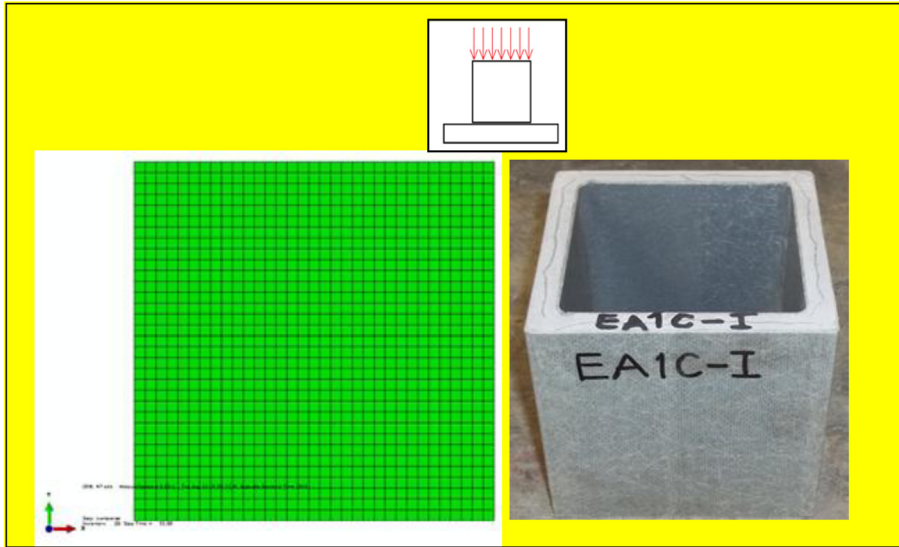


Fig. 4. Finite element mesh.

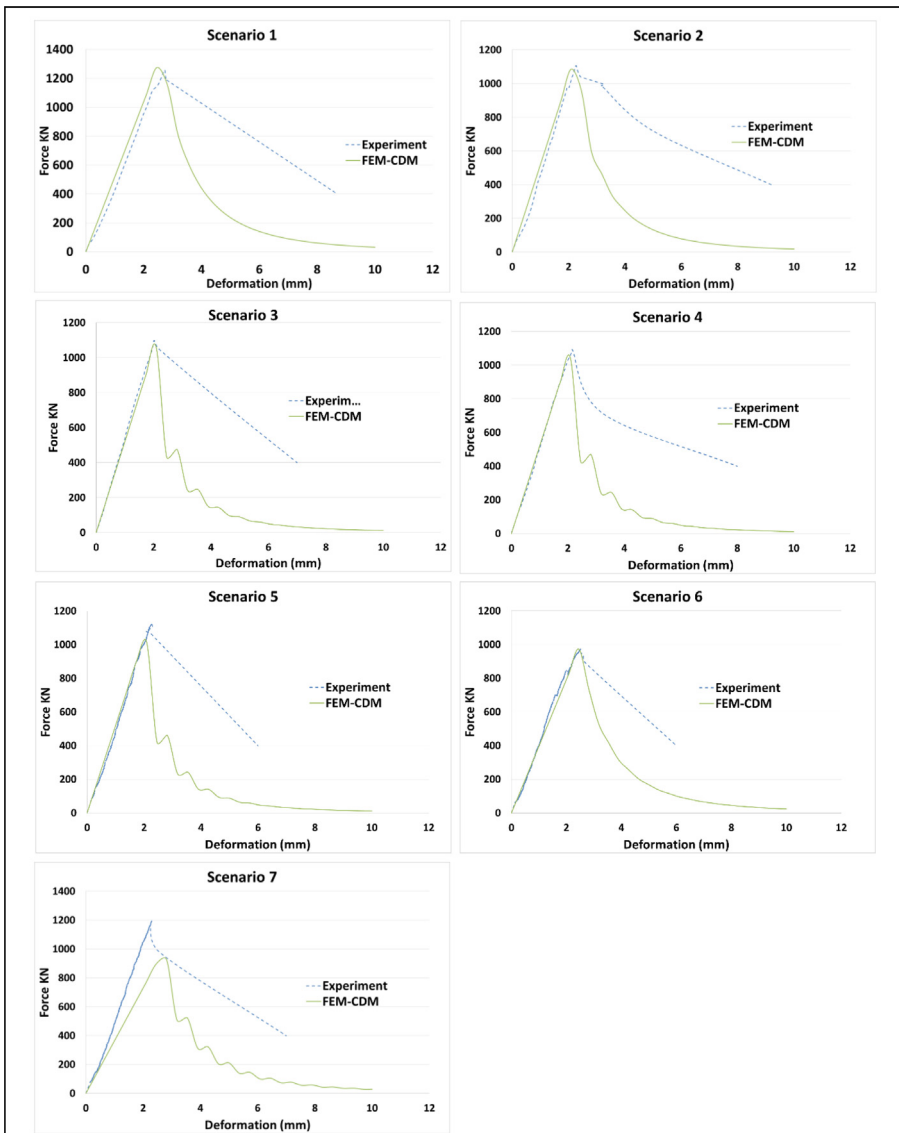


Fig. 5. Results of CMD, Simple Softening model and experiments.

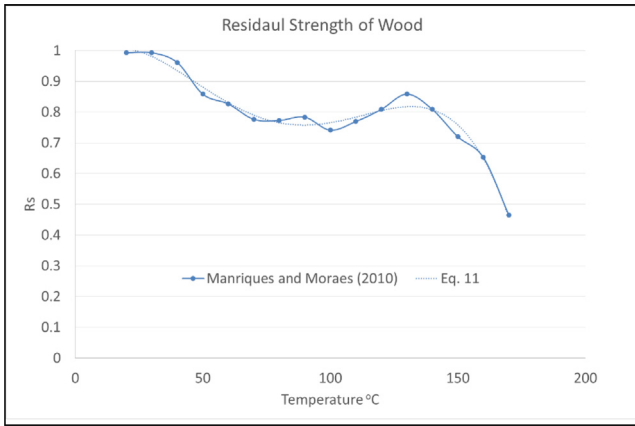


Fig. 6. Residual strength of wood according to Manriques and Moraes (2010).

Table 3
Wood material properties (From Green et al. 1999 [21]).

Property _ Wood	Notation	Value
Longitudinal tensile modulus of elasticity	E_1	9.2 (GPa)
Transverse tensile modulus of elasticity	E_2	0.589 (GPa)
Radial tensile modulus of elasticity	E_3	0.984 (GPa)
Transverse shear modulus of elasticity	G_{23}	0.258 (GPa)
In-plane shear modulus of elasticity	$G_{12} = G_{13}$	0.607 (GPa)
Major Poisson's ratio	$\nu_{12} = \nu_{31}$	0.33
Minor Poisson's ratio	ν_{23}	0.326
Bulk weight density of FRP	γ	370 (kg/m ³)
Compressive strength parallel to grain	σ_{xc}	29.9 (MPa)

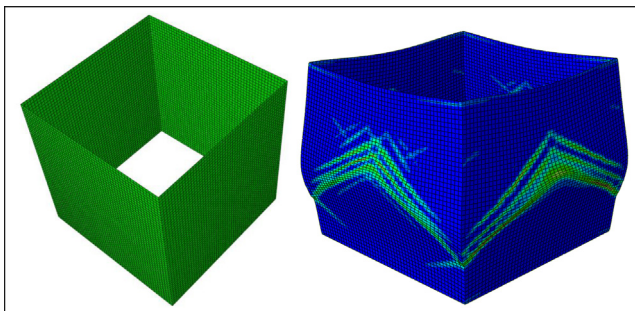


Fig. 7. Virgin and deformed mesh after collapse of wood material under compressive load.

$$R_s = 1 - \frac{0.9}{1 + \exp(-10(\frac{T}{1200} - 0.43))} \quad (12)$$

In Eq. (12), the temperature (T) can vary between 20 to 1200 °C and the R_s is the residual strength (percentage) of concrete.

The elastic modulus of concrete is known to be a function of its index of compressive stress [24]. Therefore the following equation is used to simulate the change of modulus of concrete samples according to their modified compressive strength:

$$E_c = 4700\sqrt{f'_c} \quad (13)$$

where E_c is the elastic modulus in MPa and f'_c is the specific compressive strength of concrete in MPa.

In this simulation concrete is assumed to be an isotropic homogenous material and the mechanical characteristics of NSC are stated in Table 4.

Concrete materials are known to be brittle under compressive loading. The FEM simulation predicted this characteristic increases

when the material is subjected to elevated temperatures. It should be noted that the simulation of the degradation strength of concrete has been conducted at a very high temperature (up to 1000 °C). In addition, there is a critical temperature for concrete degradation (600 °C in this simulation) after which a massive reduction in concrete strength occurs.

Fig. 11 shows the maximum load capacity of NSC samples decreases from 470 kN at room temperature to 52 kN at 1000 °C. In addition, the deformation before collapse reduces from 2.1 mm at 20 °C to 0.25 mm at 1000 °C. This suggests less ductile behaviour from NSC when subjected to higher temperatures. The results of the FEM simulations are then developed based on the experimental data published by to Chen et al. [23].

7. Simulation of strength degradation in steel with increasing temperatures

The simulation of the degradation of the compressive strength of steel with increasing temperatures is reviewed in this section. Yang and Hsu [25] presented the experimental results of the structural behaviour of centrally loaded steel columns (SN490) at elevated temperatures. Their work has been used as the basis of Eq. (14) to represent the degradation of compressive strength of steel materials at high temperatures. Fig. 12 incorporates Eq. (14) along with the experimental results of Yang and Hsu [25].

$$R_s = 1.075863 - 4.054361 \times 10^{-3}T + 1.324822 \times 10^{-5}T^2 - 1.400734 \times 10^{-8}T^3 \quad (14)$$

Similar to Section 5, a hollow square box made is simulated. The box is a cube of 10 × 10 × 10 cm and is modelled by 10,000 S8R 8 nodes shell elements. The model is under uniformly distributed compressive pressure. The steel material properties are modelled as isotropic rate dependent hardening materials [22]. Table 5 shows the mechanical properties of steel at 20 °C which are used in the simulation.

Fig. 13 shows the behaviour of steel samples (SN490) subjected to varying temperatures. The simulation has been conducted for 20 °C, 400 °C, 450 °C, 500 °C and 550 °C. It can be seen that a significant reduction occurs at 450 °C. This suggests that similar to concrete, the reduction of compressive strength in steel materials is significant when the temperature reaches a critical value (450 °C in this simulation).

Similar to NSC samples, the load capacity and ductility of the SN490 samples have reduced due to the increase in temperature.

The numerical simulation in this sections is then developed based on the experimental results of Yang and Hsu [25].

8. Discussion on the experimental results and those estimated by the predictive models

In this research different finite element constitutive models are employed to predict the behaviour of four different types of construction materials under temperature duress. The materials included GFRPs, wood, normal strength concrete and steel (SN490).

The numerical simulation of the behaviour is then developed based on experimentally published data for each specific type of material.

The mechanical behaviour of GFRPs is known as anisotropic brittle. Wood is anisotropic but can show more ductile responses before collapse. Concrete is isotropic and brittle, and steel is considered an isotropic ductile material.

The finite element model for each type of material simulated the response of the materials under compressive loading and temperature duress.

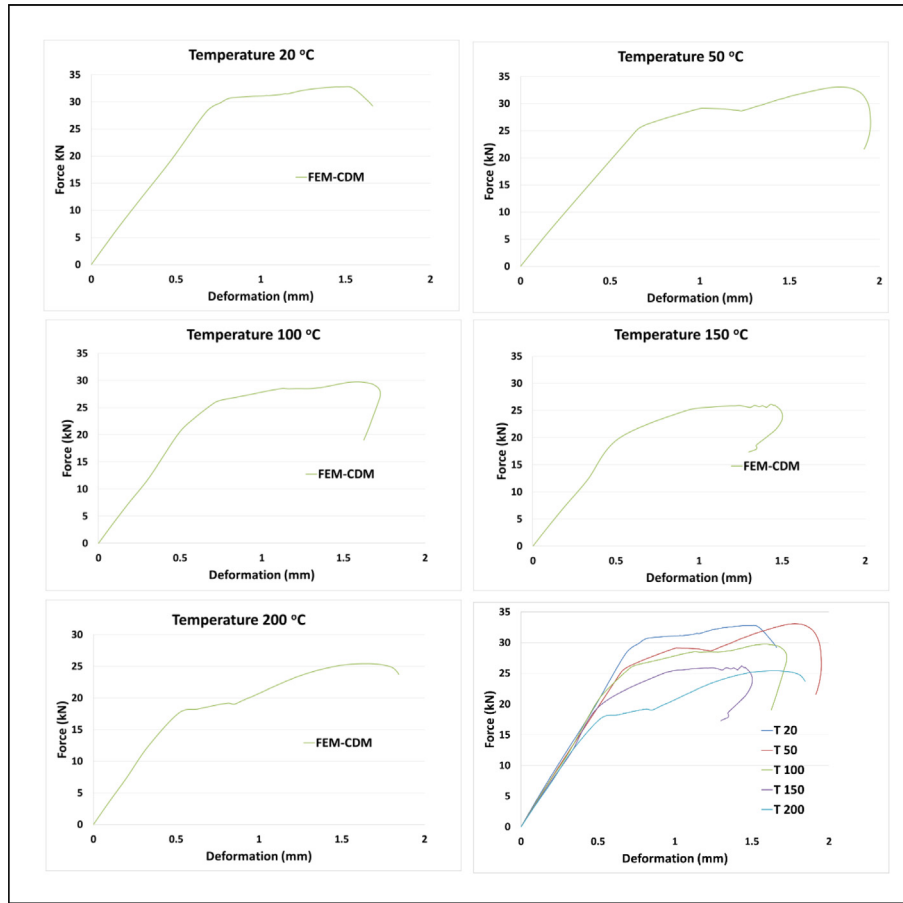


Fig. 8. Simulation of degrading compressive strength in wood under increasing temperature.

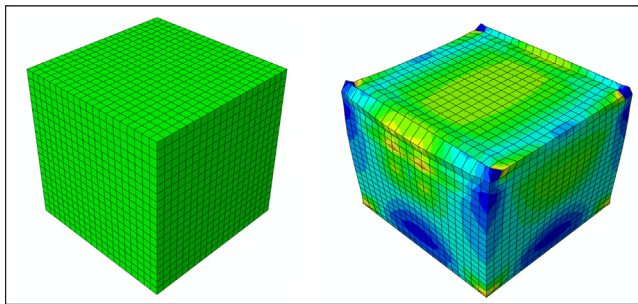


Fig. 9. Virgin and deformed mesh after collapse of a concrete cube under compressive load.

Concrete and steel show a small reduction in compressive strength up until 200 °C. However, in both of these materials there is a critical temperature after which a significant reduction occurs in load bearing capacity.

The GFRP samples lost a portion of their compressive strength, however, the strength lost is not more than 25% of the original capacity. Whilst the GFRP samples show a softening behaviour after collapse, some degree of ductility can be expected before the actual collapse. The interactive mechanism of collapse (fibre and matrix) are thought to be responsible for this ductility.

According to Fig. 5 there is a very good agreement between numerical simulation and the experimental results before the collapse. However, the behaviour of GFRPs after the collapse remains very complex. It can be seen that the GFRP behaviour is predicted differently by experimental data and numerical simulation. The

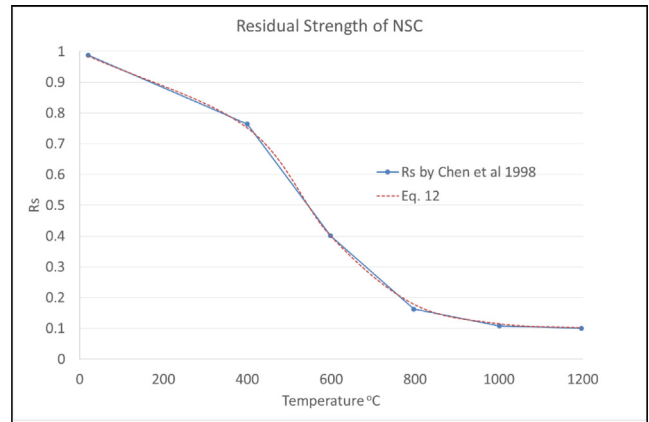


Fig. 10. Residual strength of concrete under compressive load and temperature according to Chen et al. (1998).

fact is during the experiment, the collapse of GFRPs occurred at a rate higher than assumed strain controlled conditions would

Table 4
NSC materials properties.

Property _ Concrete	Notation	Value
Modulus of elasticity	E_c	Eq. (13)
Poisson's ratio	ν	0.2
Bulk weight density of FRP	γ	2400 (kg/m ³)
compressive strength (at 20 °C)	σ_c	47.0 (MPa)

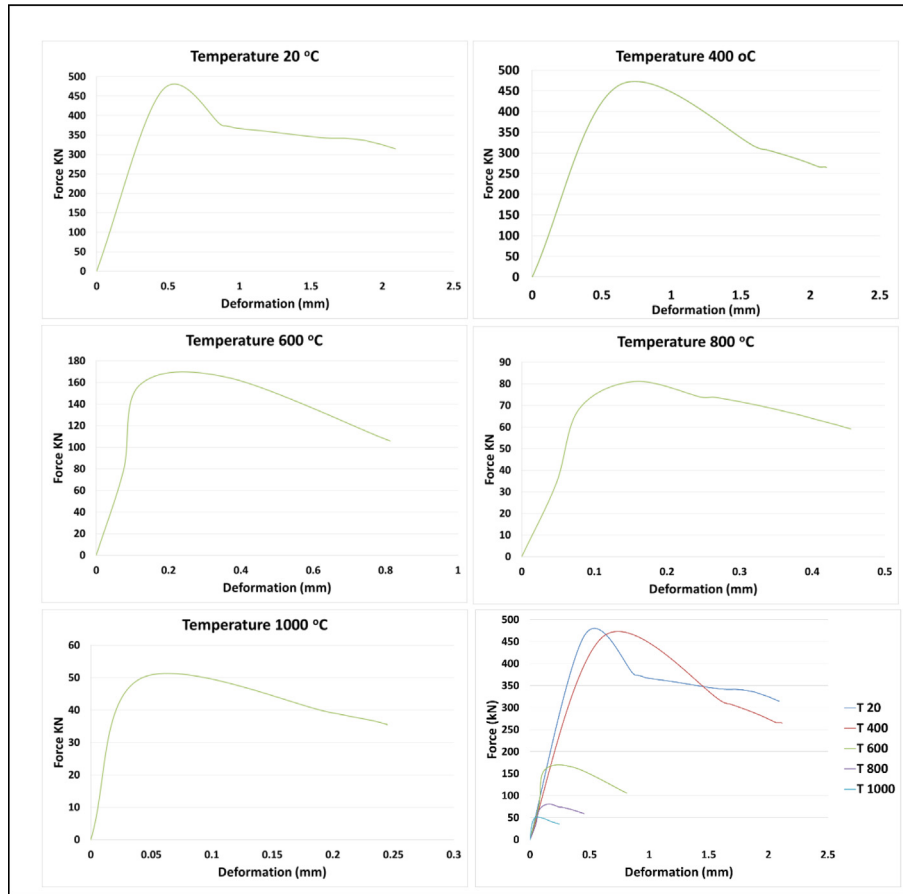


Fig. 11. Simulation of degrading compressive strength in NSC.

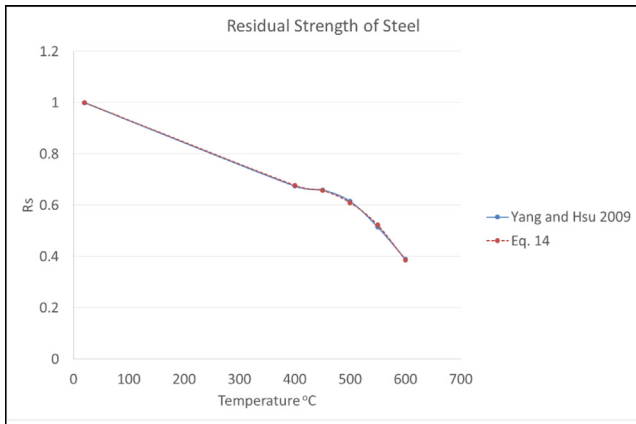


Fig. 12. Residual strength of steel according to Yang and Hsu (2009).

Table 5
Steel (SN490) materials properties.

Property _ Steel	Notation	Value
Modulus of elasticity	E	200 (GPa)
Poisson's ratio	ν	0.25
Bulk weight density of FRP	γ	2400 (kg/m ³)
Compressive strength (at 20 °C)	σ_c	343.0 (MPa)

produce and that UTM gauges would measure. On the other hand, numerical simulation assumes the material behaviour is perfectly

governed by the softening rate-dependent equations. However, this assumption might not hold entirely, as expected, in reality. Having these two points in mind, it should be quite possible that the actual failure behaviour of the samples might have a path bonded by both the curves of the experimental data and the numerical simulation. More dedicated investigation is required to determine the actual behaviour.

Table 6 presents the results of the compressive capacity for the four different materials at 20 °C and 200 °C. The results in Table 6 are based on numerical simulation detailed in the previous sections. The simulation shows that although often regarded as brittle material, GFRP can show significant deformation before the collapse load. Another important property of GFRP is its high compressive capacity before the collapse. The combination and interaction of high compressive capacity and large deformation before collapse are two significant strengths of GFRP when compared with other traditional construction materials (i.e.: wood, concrete and steel).

The strength loss of GFRP in comparison with other construction materials seems to be acceptable by comparison. GFRP exhibited reduced compressive strength from 1275.6 kN to 950.5 kN when temperatures increased from 20 to 200 °C. This is close to a 25% reduction in its ultimate load bearing capacity. The same ratio for wood, concrete and steel is 22%, 12% and 16% respectively. It should be noted that the reduced strength of GFRP material still exceeds the original strength of the other three comparative materials (GFRP: 950.7 kN in comparison with wood: 32.8 kN, concrete: 464.7kN and steel 634.3 kN).

To provide a basis for the comparison, the compressive strength of the materials is presented in Table 7.

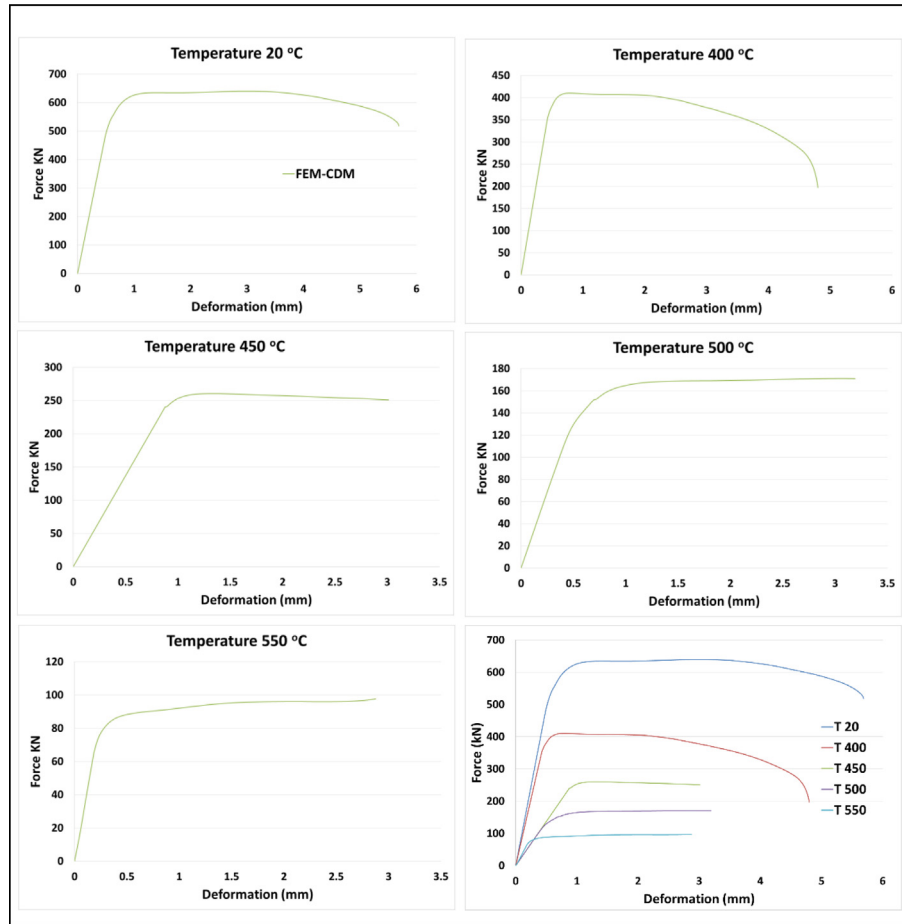


Fig. 13. Simulation of degrading compressive strength in Steel under increasing temperatures (SN490).

Table 6

Compression capacity of different materials in 20 and 200 °C.

Material	20 °C		200 °C	
	Compression Force (kN)	Final Displacement (mm)	Compression Force (kN)	Final Displacement (mm)
GFRP	1275.6	10	950.7	10
Wood	32.8	1.7	25.4	1.8
Concrete	464.7	2.1	406.6	2.1
Steel	634.3	5.7	531.9	5.3

The strength of GFRPs is higher in comparison with the other three traditional materials. This is true even after being subjected to 200 °C. GFRPs show 671 MPa and 500 MPa compressive strength at 20 °C and 200 °C respectively. It can be seen that concrete can reserve 87% of its original compressive strength after being subjected to 200 °C, whilst GFRP lost 25% of its capacity. It can be concluded that GFRPs are more sensitive to heat than concrete but the residual strength is still higher than most of the traditional construction materials investigated in this study.

Table 7

Residual strength of different materials subjected to heat.

Material	20 °C	200 °C	Residual Strength (%)
	Compression Strength (MPa)	Compression Strength (MPa)	
GFRP	671.36	500.36	75%
Wood	17.26	13.36	77%
Concrete	46.47	40.66	87%
Steel	333.84	279.94	84%

Mechanical properties of GFRP can significantly improve construction methods given the inherent high strength/weight ratio of these materials. By comparison, wood loses over 55% of its original compressive load bearing capacity and shows a notable reduction in ductility before the collapse load.

In addition, whilst GFRP is known to be higher in cost than wood, steel and concrete construction alternatives, if a whole of lifecycle building construction assessment is considered, then GFRP's durability, enhanced insulation [26] (improved energy efficiency) and lower construction costs [27] benefits are expected to lower this cost difference significantly.

9. Conclusion

In this paper the behaviour of GFRP material is compared with three traditional construction materials under compressive load and temperature duress. Different constitutive models were used to simulate the anisotropic softening behaviour of GFRPs, the anisotropic rate dependent behaviour of wood, the isotropic softening behaviour of normal strength concrete and the isotropic rate

dependent behaviour of steel. The following conclusions are proposed.

The newly developed constitutive model based on a CDM approach can successfully predict the softening brittle response of GFRPs when subjected to cycles of thermal loading and compression. The approach can calculate the reduced strength of GFRPs and predict the deformation of the materials after the collapse load.

The prediction of the reduction in compressive strength of GFRP material is based on the number of thermal cycles and the temperature peak.

The mechanical response of GFRPs to compressive loading is semi-plastic which means a significant deformation before the final collapse. This can be related to the progressive failure of the fibre/matrix composite which results in gradual collapse rather than sudden brittle failure often expected for GFRP materials.

It is interesting to note that there is a discrepancy between the numerical simulation and experimental results of GFRPs at 200 °C. The numerical simulation predicts less compressive strength than what is measured in the laboratory. Further study is required to provide better predicative capacity.

The results of the numerical simulation prove the potential long term functionality and durability of GFRPs in construction applications compared with wood, concrete and steel. The combination of GFRP's high strength and low weight ratio highlights their increasing suitability as a sustainable material option in civil construction.

GFRP materials can restore up to 75% of their original loading capacity after being subjected to temperature duress (Table 6). Increasing temperature does not decrease the ductility of GFRP materials significantly and shows a noticeable deformation before the actual collapse. The reduced strength of GFRP is comparable with the reduced strength of wood, steel and concrete materials when subjected to 200 °C.

In terms of the perceived "brittleness" of GFRP materials, the following results testify its comparative strength, ductility and durability.

Woods shows significant ductility before collapse, however, it cannot restore more than 45% of its original strength after being subjected to temperature duress. In addition, it should be noted that the actual load bearing capacity of wood is also much smaller than that of GFRP, concrete and steel.

Concrete materials are temperature resistant until critical temperatures are reached around 400 °C after which they do influence load capacity.

The strength reduction in steel is more continuous than concrete, however, like concrete, significant reductions in strength can be expected after 400 °C where a sharp reduction in both ductility and compressive capacity can be expected.

Although GFRPs lost originally available compressive capacity with the increase in temperature, the residual strength of GFRPs remains higher than the other three materials tested. This trade-off in compressive strength with increasing temperature is relative to the reduced strength of the GFRP materials.

References

- [1] Fernandez John. *Material architecture: emergent materials for innovative buildings and ecological construction*. Taylor & Francis; 2006.
- [2] Ortiz Oscar, Castells Francesc, Sonnemann Guido. Sustainability in the construction industry: A review of recent developments based on LCA. *Constr Build Mater* 2009;23(1):28–39.
- [3] Biscaia, Hugo C, Silva Manuel AG, Carlos Chastre. Influence of external compressive stresses on the performance of GFRP-to-concrete interfaces subjected to aggressive environments: an experimental analysis. *J Compos Constr* 2015;20(2):04015044.
- [4] Dentchev Nikolay, Baumgartner Rupert, Dieleman Hans, Jóhannsdóttir Lára, Jonker Jan, Nyberg Timo, et al. Embracing the variety of sustainable business models: social entrepreneurship, corporate intrapreneurship, creativity, innovation, and other approaches to sustainability challenges. *J Cleaner Prod* 2015;113:1–4.
- [5] Silva Angie, Rosano Michele, Stocker Laura, Gorissen Leen. From waste to sustainable materials management: three case studies of the transition journey. *Waste Manage* 2016.
- [6] Rosano Michele, Schianetz Karin. Measuring sustainability performance in industrial parks: a case study of the Kwinana industrial area. *Int J Sustain Dev* 2014;17(3):261–80.
- [7] Mattiussi Alessandro, Rosano Michele, Simeoni Patrizia. A decision support system for sustainable energy supply combining multi-objective and multi-attribute analysis: an Australian case study. *Decis Support Syst* 2014;57:150–9.
- [8] Sullivan K, Thomas S, Rosano M. An Industrial Ecology based view of the Firm. In: International conference on sustainable development. Columbia, New York. September 2015.
- [9] James Manyika, Michael Chui, Brad Brown, Jacques Bughin, Richard Dobbs, Charles Roxburgh, Angela Hung "Big data: The next frontier for innovation, competition, and productivity". Mckinsey Globl Institute (2011).
- [10] Ghadimi Behzad, Nikraz Hamid, Rosano Michele. Dynamic simulation of a flexible pavement layers considering shakedown effects and soil-asphalt interaction. *Transp Geotech* 2016;7:40–58.
- [11] Russo Salvatore, Ghadimi Behzad, Lawania Krishna, Rosano Michele. Residual strength testing in pultruded FRP material under a variety of temperature cycles and values. *Compos Struct* 2015;133:458–75.
- [12] Russo Salvatore, Ghadimi Behzad, Lawania Krishna, Rosano Michele. Failure analysis using acoustic and energy emission assessment of fibre reinforced polymer material performance under severe conditions. *J Reinf Plast Compos* 2016. 0731684416638552.
- [13] Perez G, Erkizia E, Gaitero JJ, Kaltzakorta I, Jimenez I, Guerrero A. Synthesis and characterization of epoxy encapsulating silica microcapsules and amine functionalized silica nanoparticles for development of an innovative self-healing concrete. *Mater Chem Phys* 2015;165:39–48.
- [14] Russo S. Experimental and finite element analysis of a very large pultruded FRP structure subjected to free vibration. *Compos Struct* 2012;94(3):1097–105.
- [15] Ahmed A, Kodur VKR. Effect of bond degradation on fire resistance of FRP-strengthened reinforced concrete beams. *Compos B Eng* 2011;42(2):226–37.
- [16] Paul Böer, Lisa Holliday, Kang Thomas H-K. Independent environmental effects on durability of fiber-reinforced polymer wraps in civil applications: a review. *Constr Build Mater* 2013;48:360–70.
- [17] CNR-DT205/2007. Guide for the design and constructions of structures made of FRP pultruded elements. National Research Council of Italy. Advisory Board on Technical Recommendations.
- [18] Barbero Ever J. *Finite element analysis of composite materials using AbaqusTM*. CRC Press; 2013.
- [19] Walter Rosen B. Tensile failure of fibrous composites. *AIAA J* 1964;2(11):1985–91.
- [20] Manríquez MJ, Moraes PD. Influence of the temperature on the compression strength parallel to grain of paricá. *Constr Build Mater* 2010;24(1):99–104.
- [21] Green, David W, Jerrold E. Winandy, David E. Kretschmann. *Wood handbook: Wood as an engineering material*. General technical report FPL-GTR-113, US Department of Agriculture, Forest Service, Forest Products Laboratory, Madison, WI, 1999.
- [22] Manual, Abaqus Users. Version 6.10-1. Dassault Systèmes Simulia Corp., Providence, RI.
- [23] Chan YN, Peng GF, Anson M. Residual strength and pore structure of high-strength concrete and normal strength concrete after exposure to high temperatures. *Cement Concr Compos* 1999;21(1):23–7.
- [24] ACI Committee 318 (2008). ACI 318–08: Building Code Requirements for Structural Concrete and Commentary. American Concrete Institute. ISBN 0-87031-264-2.
- [25] Yang Kuo-Chen, Hsu Rejia. Structural behavior of centrally loaded steel columns at elevated temperature. *J Constr Steel Res* 2009;65(10):2062–8.
- [26] Chowdhury Ershad, Bisby Luke, Green Mark, Bénichou Noureddine, Kodur Venkatesh. Heat transfer and structural response modelling of FRP confined rectangular concrete columns in fire. *Constr Build Mater* 2012;32:77–89.
- [27] Ehlen Mark A. Life-cycle costs of new construction materials. *J Infrastruct Syst* 1997;3(4):129–33.